Turkish Journal of Chemistry

http://journals.tubitak.gov.tr/chem/

Research Article

Turk J Chem
(2022) 46: 506-522

doi:10.3906/kim-2109-28

New bis-isoxazole with monoterpenic skeleton: regioselective synthesis, spectroscopic investigation, electrochemical, and density functional theory (DFT) studies

Ali OUBELLA[1,*], Meryem HRIMLA[2], Mouhi Eddine HACHIM[2], Mourad FAWZI[1], Abdoullah BIMOUSSA[1,*,], Lahoucine BAHSIS[2,3], Aziz BOUTOUIL[2], Aziz AUHMANI[1], Abdelkhalek RIAHI[4], My Youssef AIT ITTO[1,*]**

[1]Laboratory of Organic Synthesis and Physico-Molecular Chemistry, Department of Chemistry, Faculty of Sciences Semlalia, Marrakech, Morocco

[2]Laboratory of Analytical and Molecular Chemistry, Polydisciplinary Faculty, Cadi Ayyad University, Safi, Morocco

[3]Laboratory of Coordination and Analytical Chemistry (LCCA), Department of Chemistry, Faculty of Sciences of El Jadida, Chouaïb Doukkali University, El Jadida, Morocco

[4]MSO team, CNRS UMR 7312 Institute of Molecular Chemistry University of Reims Champagne-Ardenne, Bat. Europol'Agro - Moulin de La Housse UFR Sciences, Cedex 2, France

Received: 10.09.2021 • **Accepted/Published Online:** 18.12.2021 • **Final Version:** 27.04.2022

Abstract: A novel bis-isoxazole was synthesized from (R)-Carvone and p-methylbenzaldoxime, via two successive [3+2] cycloaddition reactions (**32CA**). The newly obtained bis-isoxazole has been fully characterized by HRMS and NMR spectroscopy. The HMBC experiment was performed to determine the stereo and the regioselectivity of the reaction. The electrochemical behavior of the studied compound, in oxidation and reduction processes, was examined using the cyclic voltammetry technique. In addition, the regioselectivity of the [3+2] cycloaddition reaction and the molecular structure of the title compound was performed by density functional theory (DFT). The HOMO and LUMO orbitals were investigated to determine the electronic properties of the synthesized compound. Besides, the global reactivity indexes were used to explain the regioselectivity for the formation of the bis-isoxazole, the theoretical results are in good agreement with experimental findings.

Key words: Bis-isoxazone, [3+2] cycloaddition reaction, regioselectivity, density functional theory (DFT) calculations, cyclic voltammetry

1. Introduction

Because of their heteroatomic constitution and their spatial disposition,the heterocycles have attracted much attention in innumerable fields of application [1–3], including isoxazoles especially in pharmacology, as they show various biological activities, including antioxidant [4], nematicidal [5], and antiviral [6]. Recently, isoxazoles have been widely studied as corrosion inhibitors and have revealed remarkable inhibition efficacy [7].

Among several isoxazole synthesis procedures, the [3+2] cycloaddition reactions of nitrile oxides with alkynes or alkenes can be ısed in various ways because of their straightforwardness and their efficiency [8–10]. While transition metal-mediated preparations of 3,4-disubstituted and 3,4,5-trisubstituted isoxazoles have been reported to provide remarkable yields [11-12], other efficient procedures use iodine compounds such as $PhI(OCOCF_3)_2$ [13], t-BuOI [14] or $PhI(OCOCH_3)_2$ [15-16] with oximes. Since oximes can be conveniently generated in considerable yield, the intramolecular cyclization of α,β-unsaturated oximes, or β-keto oximes constitutes the fundamental step for the successful synthesis of the isoxazole nucleus [17–18].

Nowadays, the science of molecular electrochemistry has become a crucial tool of research efforts in order to develop new renewable energy technologies that meet environmental conditions. The urgency of these environmental needs is well represented by the rapid evolution [19–23]. In the synthesis of heterocyclic compounds, organic electrochemistry is, without a doubt, one of the milder and more environmentally benign tools available to chemists [24–27]. In terms of mechanism, electrochemistry is a useful tool to examine reactions involving electron transfers or a structural modification,

* These authors contributed equally to this work.
** Correspondence: bimoussa_@hotmail.com

often resulting in the oxidation or reduction of a metal complex [28]. Among the electrochemical techniques, cyclic voltammetry is the most popular and commonly employed technique to investigate the reduction and oxidation processes of molecular species.

These bibliographic findings prompt us to expand our research work aiming at the preparation and theoretical study of heterocyclic systems with monoterpenic skeleton [29–32]. The target compound was designed by the incorporation of two isoxazole coresintoa monoterpenic skeleton by reacting (R)-carvone with an arylonitrile oxide via two sequential 1,3-dipolar cycloaddition reactions (Figure 1). Through the obtained results, we discussed the electronic and structural effects in order to carry out a comparative study of its electrochemical properties.

We report also an experimental NMR investigation of the formation of the uniquely obtained bis-isoxazole regioisomer **3**, followed by a study on the plausible mechanism for this regioselective synthesis of the stoichiometric compound **3** via the local reactivity indexes. HOMO, LUMO, and NBO analyses were performed using density-functional theory (DFT). The electrochemical activity of the studied compounds (**2** and **3)** was carried out using the cyclic voltammetry technique.

2. Experimental section

2.1. Instruments and reagents

All chemicals were used as obtained from commercial sources (Aldrich and Acros). Melting points (m.p.) were determined using a capillary apparatus and are inaccurate. Analytical thin-layer chromatography (TLC) was performed on plates precoated with E. Merck silica gel 60 F254 to a thickness of 0.25 mm. HRMS were obtained on a Q-TOF micromass spectrometer. ^{1}H and ^{13}C NMR spectra were recorded in $CDCl_3$ with a 500 MHz Bruker Avance III spectrometer with a BBFO + probe. Chemical shifts (δ) are expressed in parts per million (ppm). They were recorded relative to solvent $CDCl_3$ signal (7.26 ppm and 77.16 ppm). The (R)-carvone-isoxazole **2** was prepared according to the reported method [33].

2.2. Cyclic voltammetry

All the measurements were carried out using a potentiostat equipped with a three-electrode cell, consisting of two Pt electrodes (diameter = 0.1 cm) as working and counter-electrode as well as a saturated calomel reference electrode (SCE) (3 M KCl), all connected to a Voltalab 10 system (PGZ 100 radiometer) controlled by the Volta master 4 software. The potential was scanned between –2000mV and +2000mV at a scan rate ranging from 50 to 1000 mV/S. As the electrolyte, an anhydrous acetonitrile (CH_3CN) solution containing the synthesized compound (**2** or **3**) and tetrabutylammonium perchlorate (Et_4ClNO_4) in concentrations of 10-3 and 0.1 M, respectively was used at room temperature.

UV-Vis spectra were recorded using a UV-6300 PC double-beam spectrophotometer (200-800 nm) operating at 1 nm resolution with a scanning speed of 100 nm min-1 at room temperature. All the measurements were carried out in acetonitrile containing a concentration of 10^{-6} M for two compounds studied.

2.3. Synthesis

To a stirred solution of mono-isoxazole **2** (1eq: 6.57 mmol) and p-methyl benzaldoxime (0.5eq, 1eq: 6.57 mmol, 1.5eq, 2eq, 2.5 eq, 3eq, 3.5eq and 4eq) in CH_2Cl_2 (30 mL), aqueous NaOCl was added dropwise (during 30 min) at 0 °C (5.2%; 15.65 mmol for 1 equivalent) according to Table 1.

After stirring for 10 min (the reaction was monitored by TLC) at room temperature, the layers were separated, and the aqueous layer was extracted with CH_2Cl_2 (3 × 10 mL). The combined organic extracts were dried over anhydrous Na_2SO_4 and the solvent was evaporated in vacuo. The residue was purified by column chromatography using hexane/ Ethylacetate mixture (82:18) as eluent. The structures, spectroscopic analysis (HRMS), and the systematic name (according to IUPAC) of two products **2** and **3** are mentioned in Table 2.

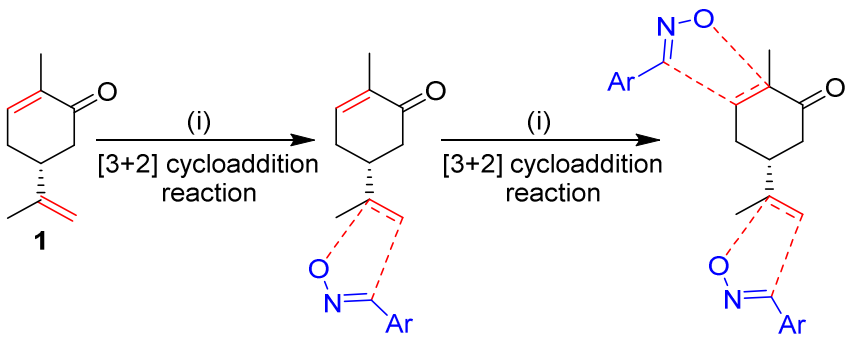

Figure 1. The design strategy of the new bis-isoxazole hybrid.

Table 1. The quantity of the volume of NaOCl added to the number of equivalents of dipole.

Number of equivalents	**0.5**	**1**	**1.5**	**2**	**2.5**	**3**	**3.5**	**4**
Volume of NaOCl (mL)	10	20	30	40	50	60	70	80
Yield obtained (%)	11	21	28	34	48	43	41	11

Table 2. IUPAC name, molecular structure, molecular formula, melting point, and analytical data of the studied isoxazole derivatives.

	IUPAC names	**Structures**	**Analytical data**
2	(R)-2-methyl-5-(5-methyl-3-(p-tolyl)-4,5-dihydroisoxazol-5-yl) cyclohex-2-en-1-one	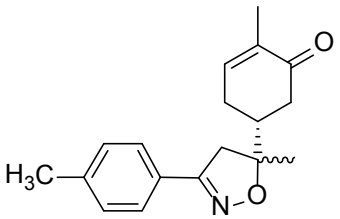	ChemicalFormula: $C_{18}H_{21}NO_2$ Exact mass: 306.1470 Molecular weight: 306.1466 Solid m.p: 96-98 °C
3	(3aS,5R,7aR)-7a-methyl-5-(5-methyl-3-(p-tolyl)-4,5-dihydroisoxazol-5-yl)-3-(p-tolyl)-3a,5,6,7a-tetrahydrobenzo[d] isoxazol-7(4H)-one	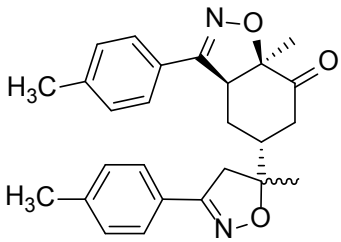	Chemical Formula: $C_{26}H_{28}N_2O_3$ Exact mass: 417.2127 Molecular weight: 417.2128 Solid m.p: 112-114 °C

(3aS,5R,7aR)-7a-methyl-5-(5-methyl-3-(p-tolyl)-4,5-dihydroisoxazol-5-yl)-3-(p-tolyl)-3a,4,5,6-tetrahydrobenzo[d]isoxazol- 7(7aH)-one (3).

Yield 11%; white solid: mp = 112±2 °C (Ethanol); HRMS (TOF-MS ES+) (m/z): found 417.2127 $[M+H]^+$, calculated 417.2128. ^{1}H NMR δ (ppm): 1.34 (3H, s); 1.42 (3H, s); 1.75 (2H, m); 1.98 (2H, m); 2.33 (3H, s); 2.28 (3H, s); 2.74-2.76 (1H, m); 2.77-3.10 (2H, m); 3.75 (1H, dd *J* = 8.75 & 1.45 Hz); 7.00-7.80 (8H, m). ^{13}C NMR δ (ppm): 20.06 (CH_3); 21.43 × 2 (2 × CH_3); 24.37 (CH_3); 26.40 (CH_2); 39.60 (CH_2); 40.09 (CH); 44.69 (CH_2); 55.60 (CH); 87.69 (C5'); 87.79 (C7a); 124.84 (CAr); 126.54 (HCAr); 126.76 (CAr); 127.76 (HCAr); 129.49 (HCAr); 129.91 (HCAr); 140.14 (CAr); 141.16 (CAr); 155.86 (C3'=N); 158.66 (C3=N); 205.83 (C=O).

2.4. Computational methods

The quantum chemical calculations were performed using GAUSSIAN 09W [34] through the DFT/B3LYP method and 6-311G(d,p) basis sets. All the frequencies obtained are positive, which proves that the structure corresponds to minimum energy [35–38]. The electronic chemical potential (μ) and chemical hardness (η) are calculated using energies of the frontier molecular orbital HOMO (E_H) and LUMO (E_L) as follows $\mu = (E_H + E_L)/2$ and $\eta = (E_L - E_H)$. The global electrophilicity (ω) and nucleophilicity (*N*) indexes were measured at the same level and are given by the following simple expressions: $\omega = \mu^2 / 2\eta$; $N = E_H - E_H$ (tetracyanoethylene (TCE)) [39-44]. The Parr functions are calculated using the Mulliken atomic spin densities [45].

3. Results and discussion

3.1. Chemistry

The first step in the synthesis of the desired hybrid bis-isoxazole **3** from (R)-carvone is the preparation of mono-adduct **2** according to the procedure reported in our previous work [33]. The second step was achieved through [3+2] cycloaddition reaction by treating the mono-adduct **2**, with a stoichiometric amount of *p*-methyl arylonitrile (generated in situ from the

corresponding oxime using 5% bleach solution). The reaction was performed at 0 °C, in dichloromethane as a solvent to yield the corresponding bis-isoxazole **3** in a high stereo and regioselective manner with low yield (11%) (Scheme1).

The low yield (11%) of the bis-isoxazole **3** has prompted us to carry out an optimization study of the reaction yield by increasing the number of equivalents of *p*-methylbenzonitrile oxide. The obtained results are shown in Table 3.

As revealed in Table 3, the yield of the reaction increases with the increase of the number of equivalents of p-methyl arylonitrile, such as the use of three equivalents of dipole gave the desired compound with an improved yield of 48 %. On the other hand, under the same operating conditions, there is a drop in yield from 48% to 41% in the case of 3.5 and 4 equivalents. This drop-in yield is likely due to the effect of the excess dipole on the formed bis-isoxazole **3**.

^{1}H NMR and ^{13}C NMR spectrum analysis of compound 3

The mono-adduct **2** was synthesized and identified according to the reported work [33]. Similarly, the newly synthesized bis-isoxazole **3** was fully characterized from its spectral NMR (1D & 2D) and HRMS data. In HRMS spectrometry, bis-isoxazole **3** reveals its pseudo molecular ion at m/z = 417.2127 $[M+H]^+$, which is consistent with the molecular formula $C_{26}H_{28}N_2O_3$. In NMR spectra of the hybrid compound **3**, and in comparison with those of starting mono-adduct **2**, we can easily state that the attack of the 1,3-dipole occurs on the internal double bond of the terpenic skeleton. Indeed, the first noteworthy data ARE the disappearance of resonances (δ ^{1}H 6.76 ppm; δ ^{13}C 144.50 ppm), characterizing the methane group (HC=) of the internal double bond of the precursor **2**. These letters are replaced in δ ^{1}H NMR spectra by one hydrogen doublet of doublet δ ^{1}H 3.75 ppm J = 1.1 & 6.8 Hz attributed to the proton at C3a position, while in ^{13}C NMR spectra, we noted two shielded signal at 55.60 and 87.79 ppm assigned respectively to C3a and C7a of isoxazole.

The 1,3-dipolar cycloaddition reaction of the 4-methylbenzonitrile oxide on the C=C dipolarophile of compound **2** can theoretically take place at both or one of its two faces according to two opposite directions leading to the formation of two possible regioisomers (**A** & **B**) each in the form of two possible diastereomers (**A**: **A1** and/or **A2**) and (**B**: **B1** and/or **B2**) (Figure 2).

To resolve this structural problem, 2D (two-dimensional) NMR spectroscopy was carried out, and HMBC (heteronuclear multiple bond correlation) experiments (Figure 3) allowed us to rule out **B1** and **B2** and confirm the **A1** or **A2** stereoisomers.

Indeed, in the HMBC spectrum (Figure 3), we note a $^{2}J_{CH}$ correlation between the C3a-H proton (δ ^{1}H 3.75) and the C3=N imine carbon (δ ^{13}C 158.66) of the isoxazole ring, while no correlation was observed between this latter and the protons of C7a-CH_3 methyl group (δ ^{1}H 1.42). This deep examination of the HMBC spectrum informs us about the

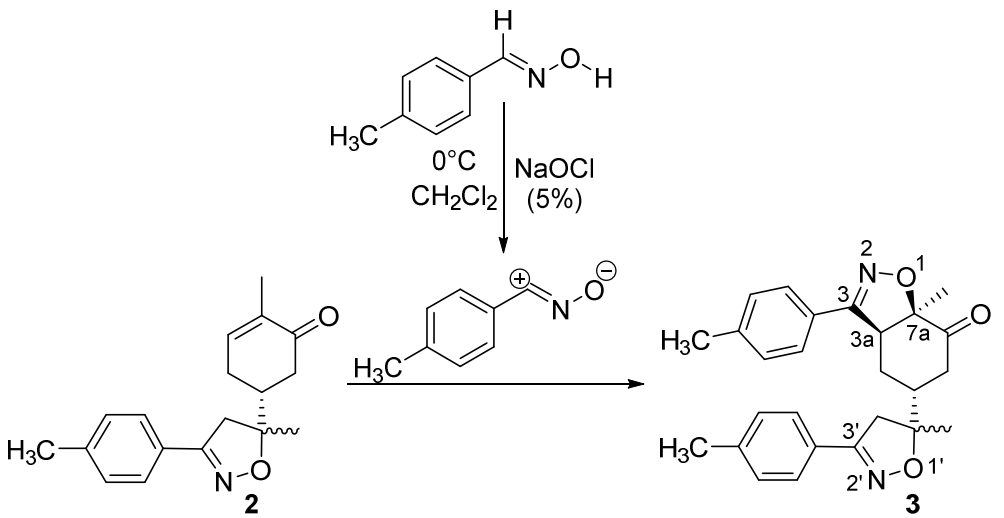

Scheme 1. Synthetic route to bis-isoxazole hybrid compound **3**.

Table 3. Effect of the 1,3-dipole amounts on the reaction yield.

Quantity of dipole (eq)	1	1.5	2	2.5	3	3.5	4
Yield (%)	11	21	28	34	48	43	39

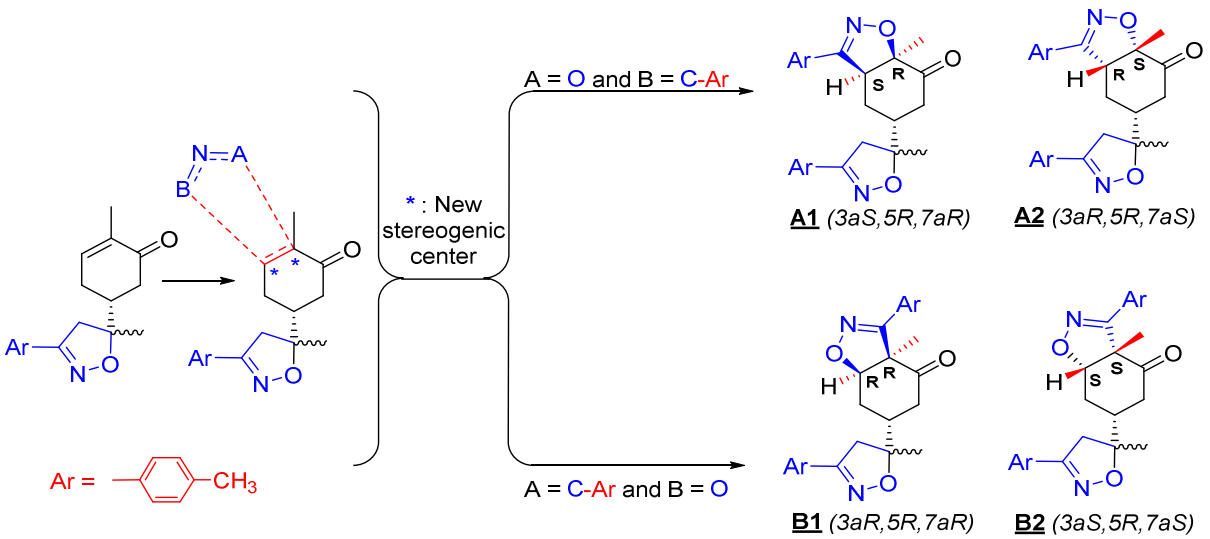

Figure 2. Selected reaction paths associated with the [3+2] cycloaddition reaction of *p*-methyl benzonitrileoxid with (R)-carvone-isoxazole **2**.

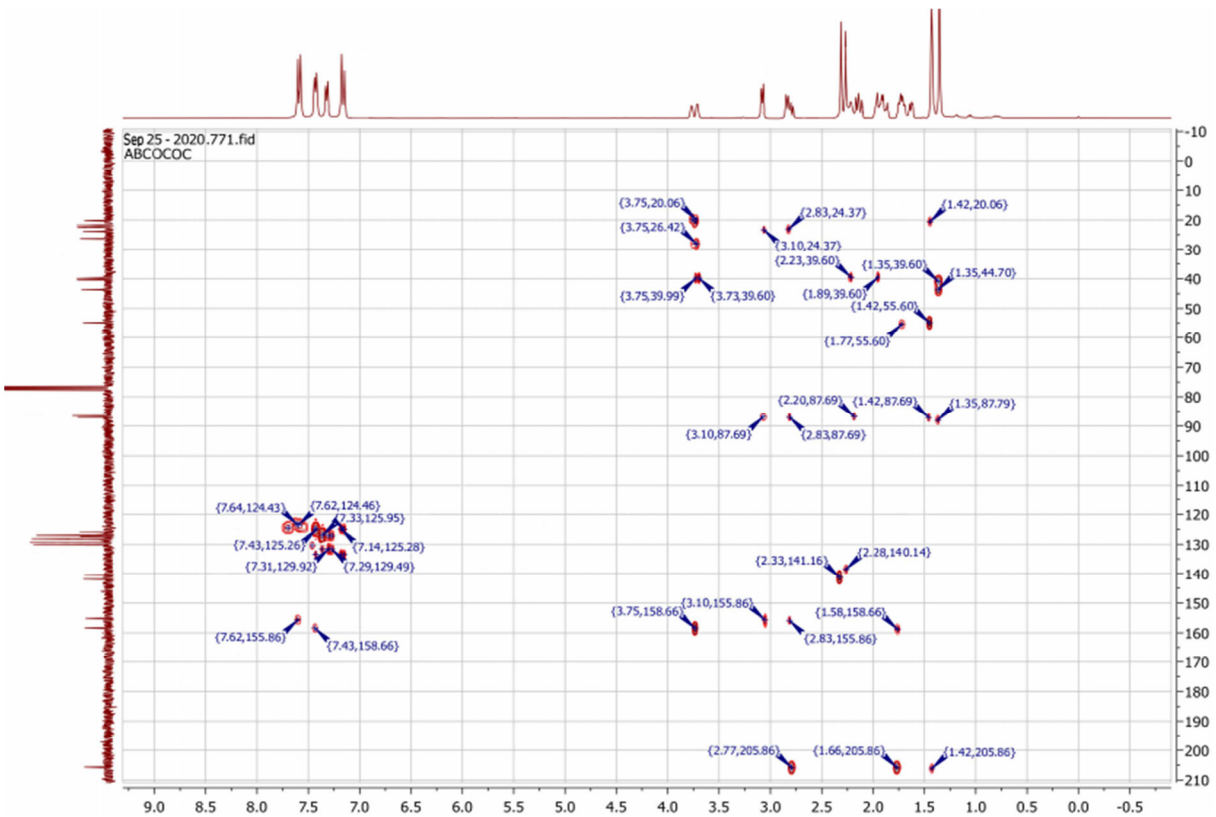

Figure 3. The HMBC correlations of bis-isoxazole-carvone **3**.

regioselective formation of isomer **A** (**A1** or **A2**) (Figure 4-A). In the same spectrum, we can also note a $^{3}J_{CH}$ correlation between the C3a-H proton (δ ^{1}H 3.75) and the methyl carbon at the C7a position. This three bond correlation would be present in both **A1** and **A2** diastereoisomers (Figure 4-B).

Thus, the 1,3-dipolar cycloaddition reaction of 4-methylbenzonitrile oxide on isoxazoline **2** was highly regioselective. This result corroborates the one obtained in our recently published study, which showed that the C3 carbon (in beta position

of the carbonyl group) is more nucleophilic than the C2 carbon (in alpha position of the carbonyl group) [45]. Therefore, the bis-isoxazoline **3** is obtained in a unique manner where the oxygen atom of the 1,3-dipole is linked to the more hindered carbon of the cyclohexenic double bond of the isoxazoline **2**. Furthermore, the 1,3-dipolar cycloaddition reaction of 4-methylbenzonitrile oxide on isoxazoline **2** was revealed to be also highly diastereoselective. This could be ascribed to the fact that the *Si* face of the cyclohexenic double bond of **2** is much more sterically hindered than the *Re* face. Therefore, the approach of the 1,3-dipole on the isoxazoline **2** should be favoured on the *Re* face thus producing the obtained **A1** diastereoisomer (Figure 5).

If the regioselectivity of the reaction was unambiguously established, its diastereoselectivity and, so, the absolute configuration of the two newly formed asymmetric carbons C3a and C7a remained unknown. In an attempt to resolve

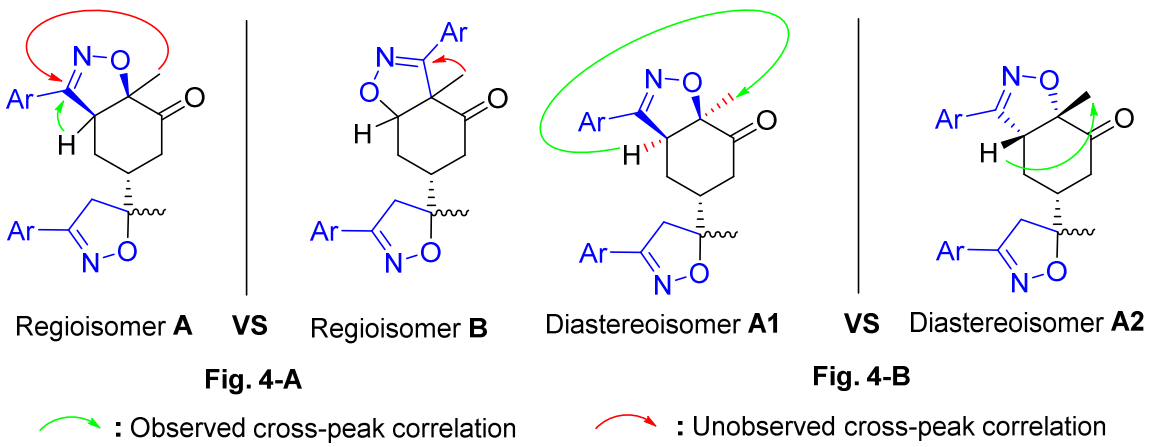

Figure 4-A, B. Main HMBC cross-peaks correlations were observed in the 2D-NMR spectra of compound **3**.

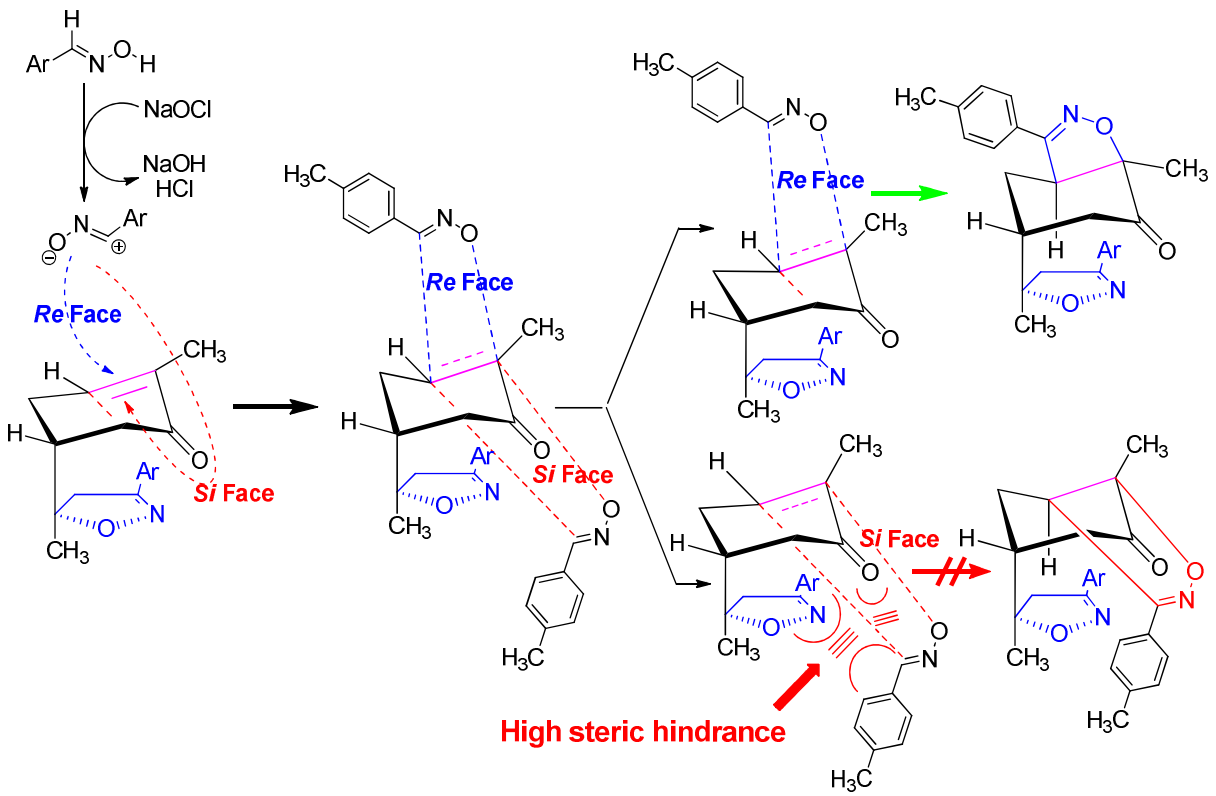

Figure 5. The proposed mechanism of the formation of the stereoisomer A1 of bis-isoxazoline 3.

this problem, we have carried out a DFT. Theoretical study where ^{1}H and ^{13}C NMR chemical shifts of compound **3** were calculated at the B3LYP/6-31G(d,p) using GIAO approach in the solvent phase. The calculations were performed in $CDCl_3$ solvent by using C-PCM formalism, and the selected shifts were compared with the experimental values as illustrated in Table 4.

According to Table 4, we can see that the highest chemical shift value was that of the carbonyl group (C7 atom), which was observed experimentally at 205.83 ppm, while the corresponding calculated values were 214.64 ppm for **A1** and 219.97 ppm for **A2**. Concerning the C8 and C9 carbon atoms of the two methyl groups, which were revealed with the lowest chemical shift values, they were observed experimentally at 20.06 and 24.37 ppm, while, theoretically, they were noted at 19.52 and 25.27 ppm for diastereomer **A1** and 17.61 and 23.01 ppm for diastereomer **A2**. A slight difference was observed between the C5' and C7a isoxazolic carbons; their experimental chemical shift values were recorded respectively at 87.69 and 87.79 ppm, while their theoretical ones were recorded at 94.51 and 92.30 ppm for **A1**, and at 95.96 and 96.33 ppm for **A2,** respectively.

Among the two Csp^3 methine groups, the one at C3a position (^{1}H 3.76, ^{13}C 55.79) is more deshielded than the one at C5 position (^{1}H 2.35, ^{13}C 39.10) because of the inductive withdrawing effect of the adjacent imine group. The calculated chemical shift values of C3a-H methine group were (^{1}H 3.59, ^{13}C 59.71) for **A1** and (^{1}H 3.41, ^{13}C 61.66) for **A2**. On the other hand, those of C5-H methine group were (^{1}H 2.24, ^{13}C 39.53) for the diastereomer **A1** and (^{1}H 1.99, ^{13}C 43.41) for the diastereomer **A2**.

The conclusion to be drawn concerning the comparability between the experimental and the theoretical findings is that the experimental NMR data are consistent with the computed values from the optimized structure of diastereomer **A1** (Figure 6).

Table 4. Experimental and theoretical (^{1}H and ^{13}C) NMR chemical shift (ppm) of studied diastereoisomers (**A1** & **A2**).

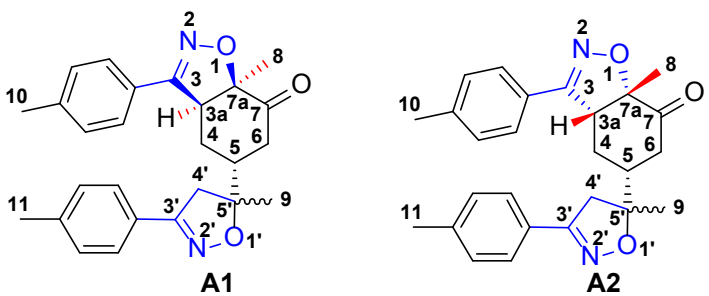

^{1}H NMR chemical shifts (ppm)				^{13}C NMR chemical shifts (ppm)			
Atoms	**Experimental ($CDCl_3$)**	**Calculated DFT/B3LYP (ppm)**		**Atoms**	**Experimental ($CDCl_3$)**	**Calculated DFT/B3LYP (ppm)**	
		A1	**A2**			**A1**	**A2**
H-4'a	2.87 3.71 2.25 1.35 3.77 1.42 2.15 2.17 1.89 2.83	2.57	1.32	C4'	44.69 87.69 87.79 21.43 21.49 20.06 24.37 55.60 155.86 158.66 205.83	41.33	39.02
H-4'b		3.02	2.82	C5'		94.51	95.26
H-5		2.45	2.46	C7a		92.30	96.33
H-9		0.94	0.23	C10		21.54	19.85
H-3a		3.59	3.41	C11		21.56	19.88
H-8		1.39	1.61	C8		19.52	17.61
H-10		2.50	1.21	C9		25.27	23.01
H-11		2.51	1.16	C3a		59.71	61.66
H-6a H-6b		1.92 2.94	1.95 1.32	C3' C3 C7		160.94 165.13 214.64	153.80 171.82 219.97

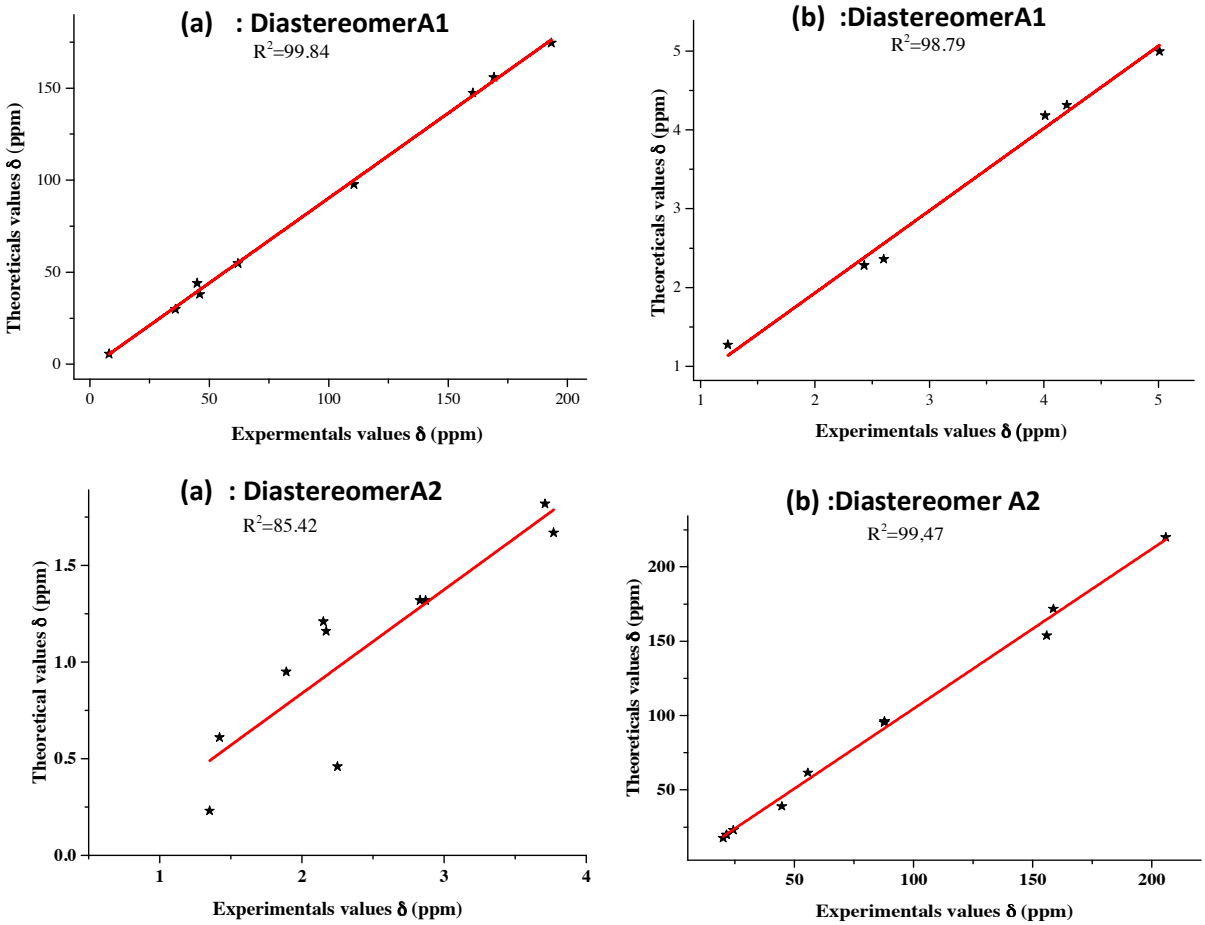

Figure 6. Correlation curves between the predicted and experimental ^{1}H NMR. (**a**) and ^{13}C NMR, (**b**) chemical shifts for product **3**.

According to this NMR analysis, which allowed an approximate assignment of each carbon and its protons, we can relatively conclude that the absolute configuration of both new stereogenic centers (C3a & C7a) is 3aS and 7aR.

3.2. IR spectral analysis

Subsequently, an FT-IR spectral study of the title compound was carried out. The structure of compound **3** was confirmed according to its IR spectral data, the existence of the band at υ_{max} = 1720 cm^{-1} corresponds to the carbonyl group (C=O). The characteristic band of the aromatic nucleus (C=C) has been revealed at 1515 cm^{-1}. However, the scaled harmonic vibrational frequencies of compound **3** were calculated from the optimized structure with DFT/B3LYP using a 6-31G(d,p) basis set at room temperature in the region between 400 and 4000 cm^{-1}. The experimental and theoretical spectrums plotted on the transmittance (%) against the wavenumber (cm^{-1}) are shown in Figure 6a,6b.

The calculated frequencies of the diastereoisomer **A1** and **A2** were compared with the observed values, and the results found are grouped in Table 5.

3.3. Mechanistic study

The geometric structure of compound bis-isoxazole hybrid **3** (**A1**) was optimized using DFT at B3LYP/6-311G(d,p) level (Figure 7).

The cycloaddition reaction of compound **2** in the presence of the 1,3-dipole is illustrated in Scheme 2. To get a closer understanding of the regioselectivity experimentally, DFT calculations were performed at the B3LYP/6-311G(d,p) level of both reagents. The optimized geometries obtained and the numbering of the atoms of the most stable conformation of both reactants are shown in Figure 8.

The global reactivity indexes are potent tools that can explain the reaction mechanism and are measured through the global electron density transfer (GEDT) value [46–47]. In this regard, the global electrophilicity and nucleophilicity indexes are calculated and summarized in Table 6. The electronic chemical potential value of dipole, μ = –3.94 eV, is closer

Table 5. Comparison of the experimental and theoretical vibrational spectra analysis of the compound. 3**.**

Assignment	**Experimental FT-IR (cm-1) with KBr**	**Calculated (cm-1) B3LYP/6-311G(d,p)**	
		A1	**A2**
υ(C-H)	3439.32	3113.07	3113.34
$\upsilon(C=O)_{Ketone}$	1720.75	1774.55	1777.19
υ(C=N)	1615.09	1655.39	1656.30
υ(C=C)	1515.09	1547.79	1547.69
υ(CH2)	1444.60	1495.13	1492.94
υ(C-C)	1358.07	1375.87	1375.32
υ(N-O)	913.94	949.21	951.27

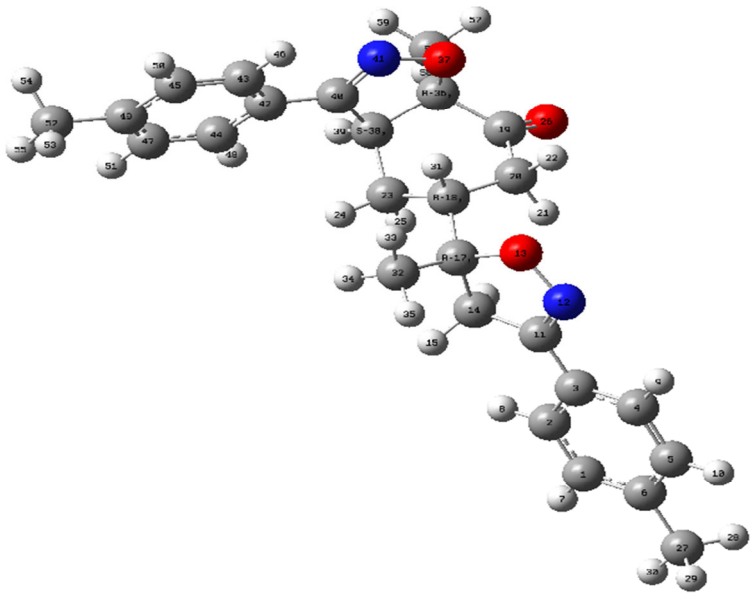

Figure 7. Optimized geometry of product **3** atB3LYP/6-311++G(d,p) level.

to that of the compound **2**, **μ** = –3.88 eV. These results confirm that this 32CA reaction will have a nonpolar character. The electrophilicity ω indices (1.63 and 1.54 eV) and the nucleophilicity N indices (2.93 and 2.65 eV) of the compound **2** and dipole illustrate that both reagents act as moderate electrophiles and moderate nucleophiles within the electrophilicity and nucleophilicity scales, confirming the nonpolar character of this cycloaddition reaction and suggests high activation energy for the formation of the corresponding products [48].

Recently, Domingo et al. have proposed the Parr functions as a helpful tool to explain the regioselectivity that is experimentally observed in 32CA reactions [49]. The authors confirmed that the ethylene group could participate in 32CA reactions by forming the first new single bond through their most electrophilic center. Therefore, the local reactivity of compound **2** was analyzed by the electrophilic P_k^+ Parr functions (Figure 9). The P_k^+ Parr function analysis indicates that the carbon C19 atom with a P_k^+ value of 0.24 is more electrophilic center than the carbon atoms C20 and C21, with P_k^+ values of 0.12 and 0.01, respectively. These results indicate that the first single bond formation will involve the most electrophilic C19 carbon explaining the experimentally observed results.

In order to illuminate the experimental results, two reaction paths associated with regioisomeric approach modes to the regio- and diastereofacial attacks for this 32CA reaction between product **2** and dipole were considered (Figure 9). The results indicate that the above-mentioned reaction paths proceed via a one-step mechanism, and the relative energies are donated in Figure 10.

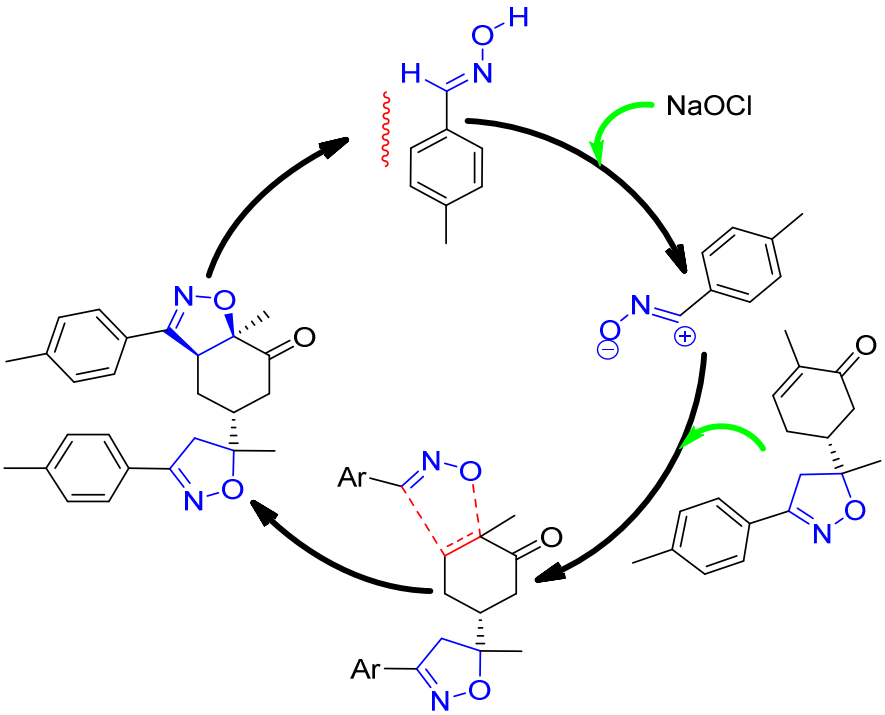

Scheme 2. The cycloaddition reaction between **2** and dipole.

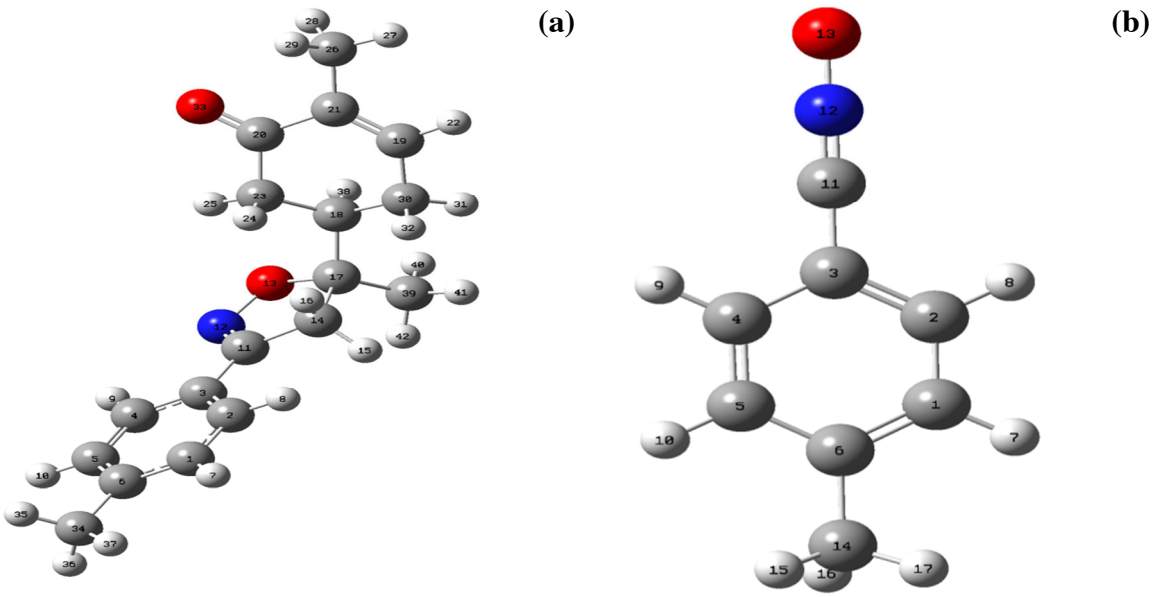

Figure 8. Optimized structures of the **2(a)** and dipole**(b)** at B3LYP/6-311G(d,p) level.

The activation energies associated with the reaction paths conduct to the formation of regioisomeric **A** are 19.09 and 20.33 kcal/mol for **A1** and **A2**, respectively. In the case of the regioisomeric **B**, the results were found to be 20.30 and 21.91 kcal/mol for the compounds **B1** and **B2**, respectively. These results confirm that the formation of the compounds **A1** and **A2** are more exothermic than the formation of **B1** and **B2**. Also, the activation energy associated with TS-A1 (1.321 kcal/mol) is lower than that associated with TS-B1. The theoretical results are in good agreement with the experimental observations (Figure 10).

Table 6. Electronics properties and global reactivity indexes of compound **2** and dipole.

	μ(eV)	η (eV)	ω (eV)	N (eV)
2	–3.88	4.62	1.63	2.93
Dipole	–3.94	5.05	1.54	2.65

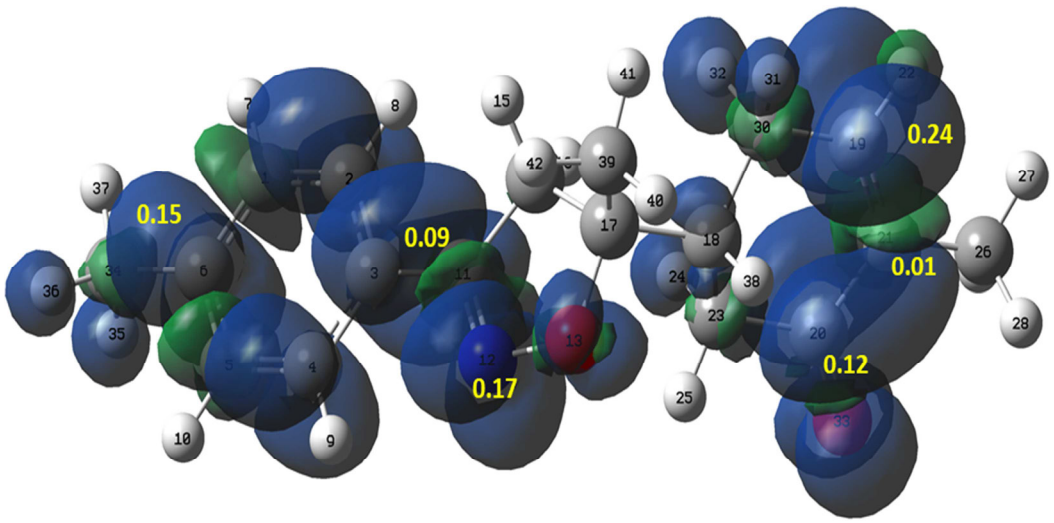

Figure 9. Three-dimensional representation of the Mulliken atomic spin densities of **2** together with the P_k^+ Parr functions values.

3.4. Electrochemistry study

3.4.1. Cyclic voltammetry measurements

The electrochemical properties of compounds **2** and **3** were performed by cyclic voltammetry in acetonitrile solution at a scan rate of 200 mV/s in the potential range from 2 to –2 V at room temperature are shown in Figure 11, and their electrochemical data are given in Table 5. The analysis of cyclic voltammetry spectra of the **2**, **3,** and their comparison with the blank spectrum show that new anodic and cathodic peaks appear as indicated in Figure 11. Indeed, the anodic current peaks observed around –1.22 and –1.48 V for compounds **2** and **3**, respectively, are located in a negative range and precede the cathodic current peaks, which appear around –1 and –1.25 V for compounds **2** and **3**, respectively; this indicates that it is not a Red/Ox system of the same grouping in the molecules, which can be explained by the irreversibility of the examined compounds [50–51]. On the other hand, these oxidation peaks observed in Figure 11 can be explained by oxidation at the α-position of the carbonyl group or/and the α-position of the double bonds, knowing that the hydrogens at these positions are labile. Then, the reduction peaks may be due to protonation of nitrogen atoms or/and reduction of nonaromatic double bonds or the carbonyl group to alcohol.

Figure 12 represents the effect of scan rate on the simulated voltammograms for 10^{-3} M of compounds **2** and **3** in a 0.1 M Et_4NClO_4/acetonitrile solution at different scan rates (50–1000 mV/s) at room temperature. The peak current intensities of both compounds increase with increasing scan rate. However, the oxidation and reduction peaks of compound **2** have the same appearance as that of compound **3,** but they move in the negative direction with a higher height of current intensities than compound **2**. This phenomenon can be attributed to the steric effect of the 5-methyl-3-p-tolyl-4,5-dihydroisoxazole group, which influences the electrochemical properties at the electrode surface.

On the other side, the HOMO, LUMO energy levels, and corresponding band gaps E_g^{CV} of the two compounds were also determined by using the cyclic voltammetry method by measuring the first oxidation (E_{ox}^{onset}) and the first reduction (E_{red}^{onset}) potentials of two studied compounds (as shown in Table 7) according to equations (1) and (2) [52–54]:

$$E_{HOMO} = -E_{ox}^{onset} - 4.8 \quad (1)$$

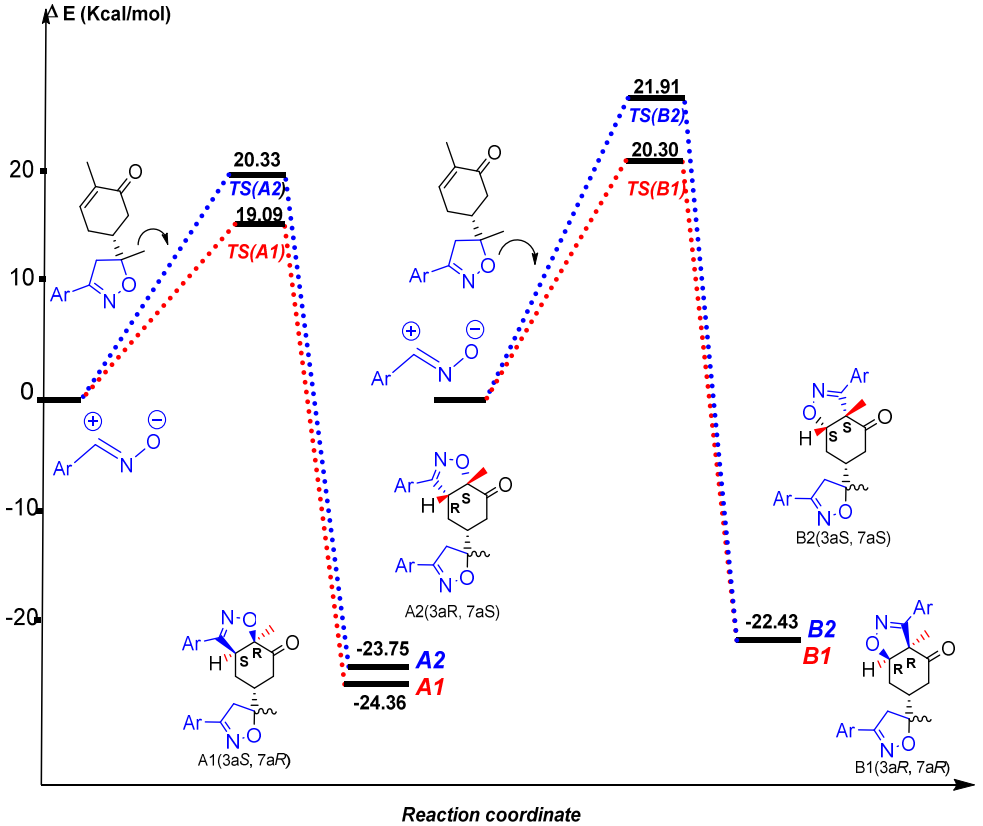

Figure 10. Relative energie for the studied reactions paths of the 32CA of benzonitrile oxide with compound **2**.

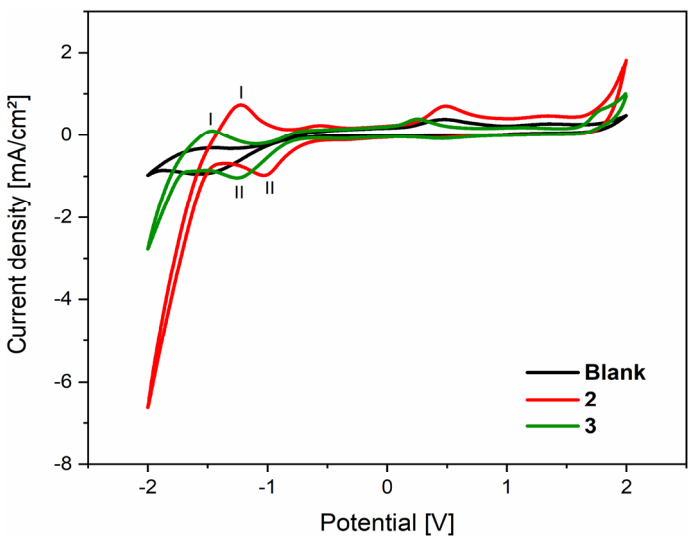

Figure 11. Cyclic voltammograms of (Black) Blank, (Red) 10^{-3}M of compound **2**, and (Green) 10^{-3} M of compound **3** in 0.1 M Et_4NClO_4/ acetonitrile solution at 200 mV/s at room temperature.

$$E_{LUMO} = -E_{red}^{onset} - 4.8 \quad (2)$$

Where (E_{ox}^{onset}) and (E_{red}^{onset}) represent the onset oxidation and reduction potential values relative to the ferrocene/ ferricenium couple, respectively with E_{ref} = –4.8 eV.

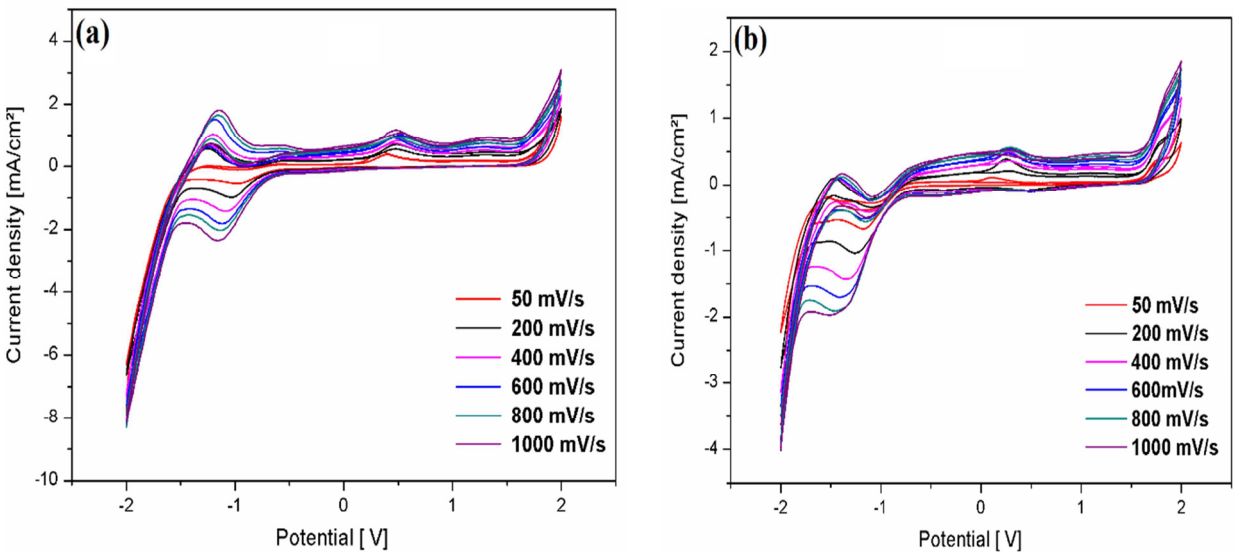

Figure 12. Cyclic voltammograms of 10^{-3} M of **2**, and **3** compounds in a solution of 0.1 M Et_4NClO_4/ acetonitrile at different scanning speeds at room temperature.

Table 7. Cyclic voltammetry parameters for the two molecules tested in a 0.1 M Et_4NClO_4 /acetonitrile solution at room temperature.

	Molecules	**2**	**3**
Oxidation Curves (I)	E_{ox}^{onset}	–1.424	–1.639
	E_{red}^{onset}	-	-
	E_{HOMO}	–3.376	–3.161
	E_g^{CV} (ev)	–1.424	–1.639
	ΔEp (mV)[(a)]	1.224	1.463
Reduction Curves (II)	E_{ox}^{onset}	-	-
	E_{red}^{onset}	–0.688	–0.808
	E_{LUMO}	–4.112	–3.992
	E_g^{CV}(ev)	0.688	3.992
	ΔEp (mV)[(a)]	1.031	1.255

(a) $\Delta E_p = \left|E_p^c - E_p^a\right|$

The band gaps E_g^{CV}were calculated from the difference between the onset of oxidation and reduction, according to the following equation [52–54]:

$$E_g^{CV} = E_{ox}^{onset} - E_{red}^{onset} \quad (3)$$

The band gaps (E_g^{CV}) of compound **3** are higher than those of compound **2**; this can be attributed to the increased size of molecule **3**. Compared to compound **2**, compound **3** has higher stability due to the lower HOMO levels. However, the LUMO energy level of compound **2** is higher than that of compound **3**, which allows for electron transfer after excitation.

3.4.2. Optical properties

The UV/Vis experimental spectra are shown in Figure 13. The maxima for compounds **2** and **3** are located in the UV-Vis at λ_{max} = 218.81; 265.19 nm (Abs = 0.2263 and 0.3427, respectively) and at λ_{max} = 220.09; 268.40 nm (Abs = 0.2402 and 0.4538, respectively), respectively. Comparing these two experimental spectra, we can note that the spectrum of compound **3** shows a slight shift and has a higher absorbance value than compound **2** due to its stronger conjugate effect [55]. This shift corresponds to an optical band gap (E_g^{Opt}) from 5.35 eV (compound **2**) to 5.37 eV (compound **3**) (Table 8). The excellent

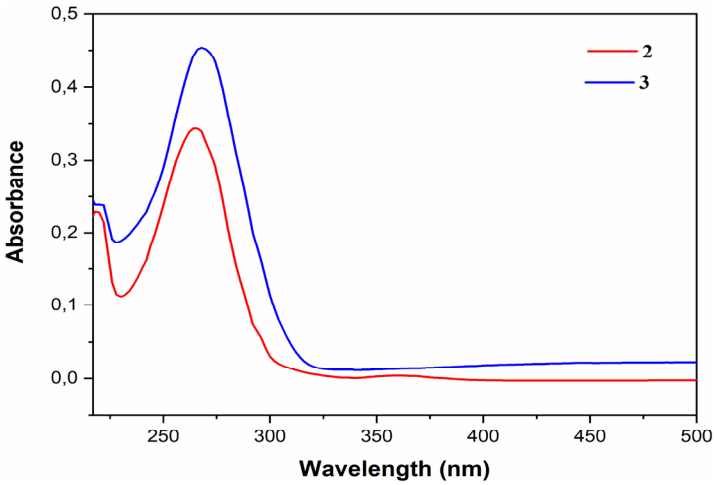

Figure 13. UV-Vis absorption spectra of compounds **2** (red) and **3** (blue) in acetonitrile at room temperature.

Table 8. Absorption edge and band gap energy of compounds **2** and **3**.

Compound	Assignments	Absorption edge (nm)	Band gap energy (E_g^{Opt} (eV))
2	π π* n π*	217.12 232.09	5.72 5.35
3	π π* n π*	217.12 231.30	5.72 5.37

absorption properties of compound **3** are associated with the large delocalization of the most occupied molecular orbital (HOMO) and the least occupied molecular orbital (LUMO) [56]. These transitions can be measured using the energy of the long-wave edge of the exciton absorption band [57]. The optical band gap (E_g^{opt}) values have been calculated according to equation (4) [58] and are presented in Table 6. However, the difference between E_g^{CV} and E_g^{Opt} is due to the progression of reduction, oxidation, and the difference in energy level between the LUMO of the electron transport units and the HOMO of hole transport units, respectively. This result has been confirmed by DFT calculations.

$$E_g(ev) = \frac{1242}{\lambda_{onset}\ (\mathrm{nm})} \tag{4}$$

4. Conclusion

In this study, we have described a synthesis of new chiral bis-isoxazole having monoterpenic skeleton, via a 1,3-dipolar cycloaddition reaction of (R)-Carvone-isoxazole with the nitrile oxide. The cycloaddition reaction was revealed to be highly regioselective. This regioselectivity was identified by a spectroscopic study of type HMBC and computational study (DFT). Cyclic voltammetry indicates that the oxidation potentials of compounds **2** and **3** vary depending upon the cycle count of the isoxazole. Moreover, DFT calculations were used to explain the regioselectivity for the formation of the bis-isoxazole, and the results are in good agreement with experimental findings.

Acknowledgments

We are grateful to Cadi Ayyad University and Chouaïb Doukkali University for providing financial support.

References

1. Bimoussa A, Oubella A, Hachim ME, Fawzi M, Ait Itto MY et al. New enaminone sesquiterpenic: $TiCl_4$-catalyzed synthesis, spectral characterization, crystal structure, Hirshfeld surface analysis, DFT studies and cytotoxic activity. Journal of Molecular Structure 2021; 1241: 130622. doi: 10.1016/j.molstruc.2021.130622

2. El Mansouri AE, Oubella A, Dânoun K, Ahmad M, Neyts J et al. Discovery of novel furo[2,3-d]pyrimidin-2-one–1,3,4-oxadiazole hybrid derivatives as dual antiviral and anticancer agents that induce apoptosis. Archiv der Pharmazie 2021; e 2100146. doi: 10.1002/ardp.202100146

3.Oubella A, El Mansouri AE, Fawzi M, Bimoussa A, Laamari Y et al. Thiazolidinone-linked1, 2, 3-triazoles with monoterpenic skeleton as new potential anticancer agents: design, synthesis and molecular docking studies. Bioorganic Chemistry 2021; 115: 105184. doi: 10.1016/j.bioorg.2021.105184

4. Padmaja A, Payani T, Dinneswara G, Padmavathi V. Synthesis, antimicrobial and antioxidant activities of substituted pyrazoles, isoxazoles, pyrimidine and thioxopyrimidine derivatives. European Journal of Medicinal Chemistry 2009; 44: 4557-4566. doi: 10.1016/j.ejmech.2009.06.024

5. Srinivas A, Nagaraj A, Reddy CS. Synthesis and in vitro study of methylene-bis-tetrahydro[1,3]thiazolo[4,5-c]isoxazoles as potential nematicidal agents. European Journal of Medicinal Chemistry 2010; 45: 2353-2358. doi: 10.1016/j.ejmech.2010.02.014

6. Egorova A, Kazakova E, Jahn B, Ekins S, Makarov V et al. Novel pleconaril derivatives: Influence of substituents in the isoxazole and phenyl rings on the antiviral activity against enteroviruse. European Journal of Medicinal Chemistry 2020; 188: 112007. doi: 10.1016/j.ejmech.2019.112007

7. Yıldırım A, Çetin M. Synthesis and evaluation of new long alkyl side chain acetamide, isoxazolidine and isoxazoline derivatives as corrosion inhibitors. Corrosion Science 2008; 50 (1): 155–165. doi: 10.1016/j.corsci.2007.06.015

8. Feddouli A, Ait Itto MY, Ait Ali M, Hasnaoui A, Riahi A. Efficient Approach for the Synthesis of Novel Functionalized Isoxazolines from Limonene. Synthetic Communications 2007; 38: 17. doi: 10.1080/00397910600943709

9. Oubella A, Ait Itto MY, Auhmani Az, Riahi A, Daran JC et al. Crystal structure of (R)-5-[(R)-3-(4-chlorophenyl)-5-methyl4,5-dihydroisoxazol-5-yl]-2-methylcyclohex-2-enone. Acta Cryst, E76 2020; 400–403. doi: 10.1107/S2056989020001991

10. Taia A, Essaber M, Oubella A, Aatif A, Bodiguel J et al. Synthesis, characterization, and biological evaluation of new heterocyclic systems 1,2,3-triazole-isoxazoline from eugenol by the mixed condensation reactions, Synthetic Commun 2020; 50: 13. doi: 10.1080/00397911.2020.1762224

11. Himo F, Lovell T, Hilgraf R., Rostovtsev V, Noodleman L et al. Copper(I)-Catalyzed Synthesis of Azoles. DFT Study Predicts Unprecedented Reactivity and Intermediates. Journal of the American Chemical Society 2005; 127 (1): 210–216. doi: 10.1021/ja0471525

12. Grecian S, Fokin VV. Angewandte, Ruthenium-Catalyzed Cycloaddition of Nitrile Oxides and Alkynes: Practical Synthesis of Isoxazoles. Chemie International Edition 2008; 47: 8285–8287. doi: 10.1002/ange.200801920

13. Jawalekar AM, Reubsaet E, Rutjes FP, van Delft FL. Synthesis of isoxazoles by hypervalent iodine-induced cycloaddition of nitrile oxides to alkynes. Chemical Communication 2011; 47 (11): 3198. doi: 10.1039/C0CC04646A

14. Minakata S, Okumura S, Nagamachi T, Takeda Y. Generation of nitrile oxides from oximes usingt-buoi and their cycloaddition. Journal of Organic Chemistry Organic Letters 2011; 13 (11): 2966–2969. doi: 10.1021/ol2010616

15. Jen T, Mendelsohn BA, Ciufolini MA. Oxidation of α-Oxo-Oximes to Nitrile Oxides with Hypervalent Iodine Reagents 2011; 76 (2): 728–731. doi: 10.1021/jo102241s

16. Mendelsohn B, Lee AS, Kim S, Teyssier F, Aulakh SV, Ciufolini MA. Oxidation of oximes to nitrile oxides with hypervalent iodine reagents. Organic Letters 2009; 11 (7): 1539–1542. doi: 10.1021/ol900194v

17. Tang SB., He JM, Sun YQ, He L, She XG. Efficient and regioselective synthesis of 5-hydroxy-2-isoxazolines: Versatile synthons for isoxazoles, β-Lactams, and γ-Amino Alcohols. Journal of Organic Chemistry 2010; 75: 1961-1966. doi: 10.1021/jo1000065

18. Heravi M, Derikvand F, Haeri A, Oskooie HA, Bamoharram FF. Heteropolyacids as Green and Reusable Catalysts for the Synthesis of Isoxazole Derivatives. Synthetic Communications 2007; 38 (1): 135–140. doi: 10.1080/00397910701651326

19. Zoski CG. Ed. Handbook of Electrochemistry; Elsevier: Amsterdam, The Netherlands 2006.

20. Bard JA, Faulkner LR. Electrochemical Methods: Fundamentals and Applications, 2nd ed.; John Wiley & Sons: Hoboken, NJ, 2001.

21. Graham DJ. Standard Operating Procedures for Cyclic Voltammetry. https://sop4cv.com/index.html 2017.

22. Ventura K, Smith MB, Prat JR., Echegoyen LE, Villagran DJ. Introducing students to inner sphere electron transfer concepts through electrochemistry studies in diferrocene mixed-valence systems. Journal of Chemical Education 2017; 94 (4): 526–529. doi: 10.1021/acs.jchemed.6b00642

23. Hendel SJ, Young ER. Introduction to electrochemistry and the use of electrochemistry to synthesize and evaluate catalysts for water oxidation and reduction. Journal of Chemical Education 2016; 93 (11): 1951-1956. doi: 10.1021/acs.jchemed.6b00230

24. Yoshida JI, Kataoka K, Horcajada R, Nagaki A. Modern strategies in electroorganic synthesis, chemcal. Reviews 2008; 108: 2265-2299. doi: 10.1021/cr0680843

25. Francke R, Little R.D. Redox catalysis in organic electrosynthesis: basic principles and recent developments Little. Chemical Society Reviews 2014; 43: 2492-2521.

26. Ma HY,. Zha ZG, Zhang Z.L, Li M, Wang ZY. Electrosynthesis of oxadiazoles from benzoyl hydrazines. Chinese. Chemical. Letters 2013; 24: 780-782. doi: 10.1016/j.cclet.2013.05.032

27. Kim BH, Jun YM, Choi YR, Lee DB, Baik W. Heterocycles. Electrochemical synthesis of 2,1-benzisoxazoles by controlled potential cathodic electrolysis. Heterocycles 1998; 48: 749-754.

28. Elgrishi N, Rountree KJ, McCarthy BD, Rountree ES, Eisenhart T et al. A practical beginner's guide to cyclic voltammetry. Journal Chemistry. Education 2018; 95: 197−206. doi: 10.1021/acs.jchemed.7b00361

29. Oubella A, Fawzi M, Auhmani A, Riahi A, Morjani H et al. Synthesis and antitumor activity of novel heterocyclic systems with monoterpenic skeleton combining dichlorocyclopropane and 1,3,4-thiadiazole nucleus. Chemistry Select 2020; 5: 6403–6406. doi: 10.1002/slct.202001284

30. Hachim ME, Oubella A, Byadi S, Fawzi M, Laamari Y et al, Newly synthesized (R)-carvone-derived 1,2,3-triazoles: structural, mechanistic, cytotoxic and molecular docking studies. Journal of Biomolecular Structure and Dynamics, 2021; 1-14. doi: 10.1080/07391102.2021.1894984

31. Laamari Y, Oubella A, Bimoussa A, El Mansouri AE, Ketatni EM et al. Design, hemiysnthesis, crystal structure and anticancer activity of 1, 2, 3-Triazoles derivatives of Totarol. Bioorganic Chemistry, 2021; 115: 105165. doi: 10.1016/j.bioorg.2021.105165

32. Bimoussa A, Oubella A, Laamari Y, Fawzi M, Hachim ME et al. Hybrid of the 1,2,3-triazole nucleus and sesquiterpene skeleton as a potential antitumor agent: Hemisynthesis, Molecular structure, Hirshfeld surface analysis, DFT, in vitro cytotoxic and apoptotic effects. Journal of Heterocyclic Chemistry 2021. doi: 10.1002/jhet.4359

33. Oubella A, Ait Itto MY, Auhmani A, Riahi A, Robert A et al. Diastereoselective synthesis and cytotoxic evaluation of new isoxazoles and pyrazoles with monoterpenic skeleton. Journal of Molecular Structure 2019; 119: 8126924. doi: 10.1016/j.molstruc.2019.126924

34. Frisch MJ, Trucks GW, Schlegel HB, Scuseria GE, Robb MA et al. Gaussian 09, Gaussian Inc, Wallingford CT 2009.

35. Singh G, Sachdeva R, Rai B, Saini GSS. Structure and vibrational spectroscopic study of alpha-tocopherol. Journal of Molecular Structure 2017; 1144:347–354. doi: 10.1016/j.molstruc.2017.05.037

36.Hachim ME, Sadik K, Byadi S, Van Alsenoy C, Aboulmouhajir A. Initio study on the six lowest energy conformers of iso-octane: conformational stability, barriers to internal rotation, natural bond orbital and first-order hyperpolarizability analyses, UV and NMR predictions, spectral temperature sensitivity, and scaled vibrational assignment. Journal of Molecular Modeling 2019; 8 (25): 1-19. doi: 10.1007/s00894-019-4105-5

37. Hachim ME, Sadik K, Byadi S, Aboulmouhajir. Electronic investigation and spectroscopic analysis using DFT with the long-range dispersion correction on the six lowest conformers of 2.2. 3-trimethyl pentane. Journal of Molecular Modeling 2020; 26: 1-16. doi: 10.1007/s00894-020-04430-4

38.Sadik K., Byadi S, Hachim ME, Aboulmouhajir A. Quantum and dynamic investigations of Complex iron-alkaloid-extract Cytisine derivatives of Retama monosperma (L.) Boiss. Seeds as eco-friendly inhibitors for Mild steel corrosion in 1M HCl. Journal of Molecular Structure 2021; 130921. doi: 10.1016/j.molstruc.2021.130921

39. Geerlings P, De Proft F, Langenaeker W. Conceptual density functional theory. Chemical Reviews 2009; 103: 1793–1874. doi: 10.1021/cr990029p

40. Domingo LR, Ríos-Gutiérrez M, Pérez P. Applications of the conceptual density functional theory indices to organic chemistry reactivity. Molecules 2016; 21. doi: 10.3390/molecules21060748

41. Domingo LR. A new C–C bond formation model based on the quantum chemical topology of electron density. RSC Advances 2014; 4: 32415–32428. doi: 10.1039/C4RA04280H

42. Sadik K, Hamdani NE, Hachim M, Byadi S, Bahadur I et al. Towards a theoretical understanding of alkaloid-extract Cytisine derivatives of Retama monosperma (L.) Boiss. Seeds, as eco-friendly inhibitor for carbon steel corrosion in acidic 1M HCl solution. Journal of Theoretical and Computational Chemistry 2020; 19; 05: 2050013. doi: 10.1142/S0219633620500133

43. Sadik K, Byadi S, Hachim ME, El Hamdani N, Podlipnik Č et al. Multi-QSAR approaches for investigating the relationship between chemical structure descriptors of Thiadiazole derivatives and their corrosion inhibition performanc. Journal of Molecular Structure 2021; 1240: 130571. doi: 10.1142/S0219633620500133

44. Moussaoui O, Byadi S, Hachim ME, Sghyar R, Bahsis L et al. Selective synthesis of novel quinolones-amino esters as potential antibacterial and antifungal agents: Experimental, Mechanistic study, Docking, and Molecular Dynamic Simulations. Journal of Molecular Structure 2021; 1224: 130652. doi: 10.1016/j.molstruc.2021.130652

45. Ríos-Gutiérrez M, Domingo LR, Esseffar M, Oubella A, Ait Itto MY. Unveiling the different chemical reactivity of diphenyl nitrilimine and phenyl nitrile oxide in [3+2] cycloaddition reactions with (R)-carvone through the molecular electron density theory. Molecules 2020; 25: 1085. doi: 10.3390/molecules25051085

46. Rachedi KO, Ouk TS, Bahadi R, Bouzina A, Djouad SE et al. Synthesis, DFT and POM analyses of cytotoxicity activity of α-amino phosphonates derivatives: Identification of potential antiviral O,O-pharmacophore site. Journal of Molecular Structure 2019; 1197: 196–203. doi: 10.1016/j.molstruc.2019.07.053

47.Uzun S, Esen Z, Koç E, Usta NC, Ceylan M. Experimental and density functional theory (MEP, FMO, NLO, Fukui functions) and antibacterial activity studies on 2-amino-4- (4-nitrophenyl) -5,6-dihydrobenzo [h] quinoline-3-carbonitril. Journal of Molecular Structure 2019; 1178:450–457. doi: 10.1016/j.molstruc.2018.10.001

48. Aurell MJ, Domingo LR, Pérez P. Contreras RA theoretical study on the regioselectivity of 1,3-dipolar cycloadditions using DFT-based reactivity indexes. Tetrahedron 2004; 60: 11503–11509. doi: 10.1016/j.tet.2004.09.057

49. R. SMITH. Characterisation and Surface Modification of Graphitic Felts. Thèse de doctorat. The University of Liverpool.2018.

50. Pamuk D,Taşdemir İH, Ece A, Canel E, Kılıç E. Redox pathways of aliskiren based on experimental and computational approach and its voltammetric determination. Journal of the Brazilian Chemical Society 2013; 24 (8): 1276-1286. doi: 10.5935/0103-5053.20130162

51. Fawzi M, Laamari Y, Koumya Y, Oubella A, Auhmani A al. Electrochemical and theoretical studies on the corrosion inhibition performance of some synthesized D-Limonene based heterocyclic compounds. Journal of Molecular Structure 2021; 124: 4130957. doi: 10.1016/j.molstruc.2021.130957

52. Ma CQ, Fonrodona M, Schikora MC, Wienk MM, Janssen RAJ et al. Solution-processed bulk-heterojunction solar cells based on monodisperse dendritic oligothiophene. Advanced Functional Materials 2008; 8 (20): 3323–3331. doi: 10.1002/adfm.200800584

53. Deshapande N, Pujar GH, Sunagar MG, Gaonkar S, Belavagi NS et al. Synthesis and optoelectronic exploration of highly conjugated 1,3,4-oxadiazole containing donor-p-acceptor chromophores. ChemistrySelect 2017; 2 (5): 1793–1801. doi: 10.1002/slct.201700048

54. Bimoussa A, Koumya Y, Abouelfida A, Ait Itto MY, Benyaich A et al. Hemisynthesis, crystal structure and inhibitory effect of sesquiterpenic thiosemicarbazones and thiazolidin-4-ones on the corrosion behaviour of stainless steel in 1 M H_2SO_4 solution. Acta Crystallographica Section C: 2019; 75: 2670-2676. doi: 10.1107/S2053229619005631

55. Rathore V, Kumar S. Visible-light-induced metal and reagent-free oxidative coupling of sp^2 C–H bonds with organo-dichalcogenides: synthesis of 3-organochalcogenyl indole. Green Chemistry 2019; 21 (10): 2670-2676. doi: 10.1039/C9GC00007K

56. Darijani NS, Modarresi-Alam AR, Noroozifar M, Hadavi SM. Single-layer solar cell based on nanostructure of polyaniline on fluorine-doped tin oxide: a simple, low-cost and efficient FTO │ n-PANI │ Al cel. Journal of the Iranian Chemical Society 2018; 15 (4): 967-980. doi: 10.1007/s13738-018-1294-2

57. Deshapande N, Pujar GH,. Sunagar MG, Gaonkar S, Belavagi NS et al. Synthesis and optoelectronic exploration of highly conjugated 1, 3, 4-oxadiazole containing donor-π-acceptor chromophores. ChemistrySelect 2017; 2 (5); 1793–1801. doi: 10.1002/slct.201700048

58. Anand S, Muthusamy A. Synthesis, characterization, electrochemical, electrical, thermal and ESIPT behaviour of oligobenzimidazoles of certain substituted benzimidazole carboxylic acids and their diode applications. Journal of Molecular Structure 2019; 1177: 78-89. doi: 10.1016/j.molstruc.2018.09.045

New bis-isoxazole with monoterpenic skeleton: Regioselective Synthesis, Spectroscopic investigation, Electrochemical, and DFT studies

Ali Oubella [1,*], Meryem Hrimla [2], Mouhi Eddine Hachim [2], Mourad Fawzi [1], Abdoullah Bimoussa[1,*], Lahoucine Bahsis[2,3], Aziz Boutouil [2], Aziz Auhmani [1], Abdelkhalek Riahi [5], My Youssef Ait Itto [1,*].

*Corresponding author:

Abdoullah Bimoussa : bimoussa_@hotmail.com,

Ali Oubella: Email address- oubellaali1@gmail.com,

My Youssef Ait Itto: Email address- aititto@uca.ac.ma

Graphical Abstract

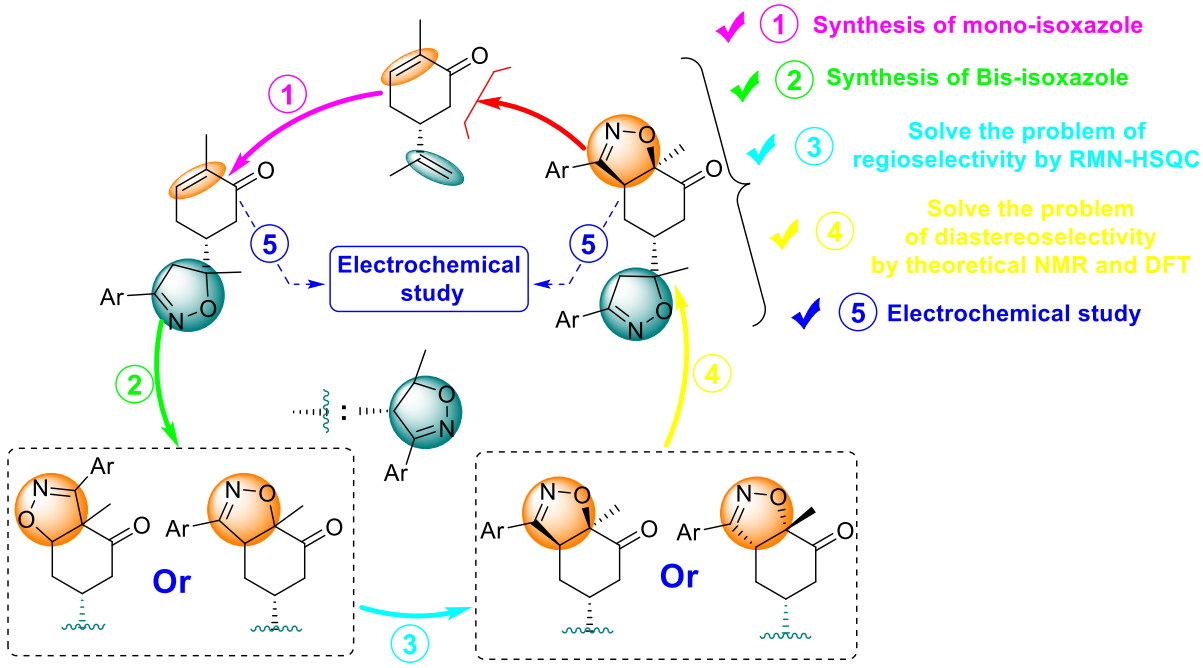

Abstract

A novel bis-isoxazole was synthesized from (R)-Carvone and p-methylbenzaldoxime, via two successive [3+2] cycloaddition reactions. The newly obtained bis-isoxazole has been fully characterized by HRMS and NMR spectroscopy. The HMBC experiment was performed to determine the stereo and the regioselectivity of the reaction. The electrochemical behavior of the studied compound, in oxidation and reduction processes, was examined using the cyclic voltammetry technique. In addition, the regioselectivity of the [3+2] cycloaddition reaction and the molecular structure of the title compound were performed by Density Functional Theory (DFT). The HOMO and LUMO orbitals were investigated to determine the electronic properties of the synthesized compound. Besides, the global reactivity indexes were used to explain the

regioselectivity for the formation of the bis-isoxazole, the theoretical results are in good agreement with experimental findings.

Spectral data for Bis-isoxazole 3:

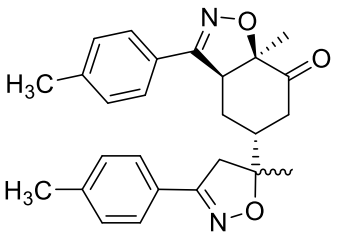

NMR Spectroscopy (500 MHz, $CDCl_3$)

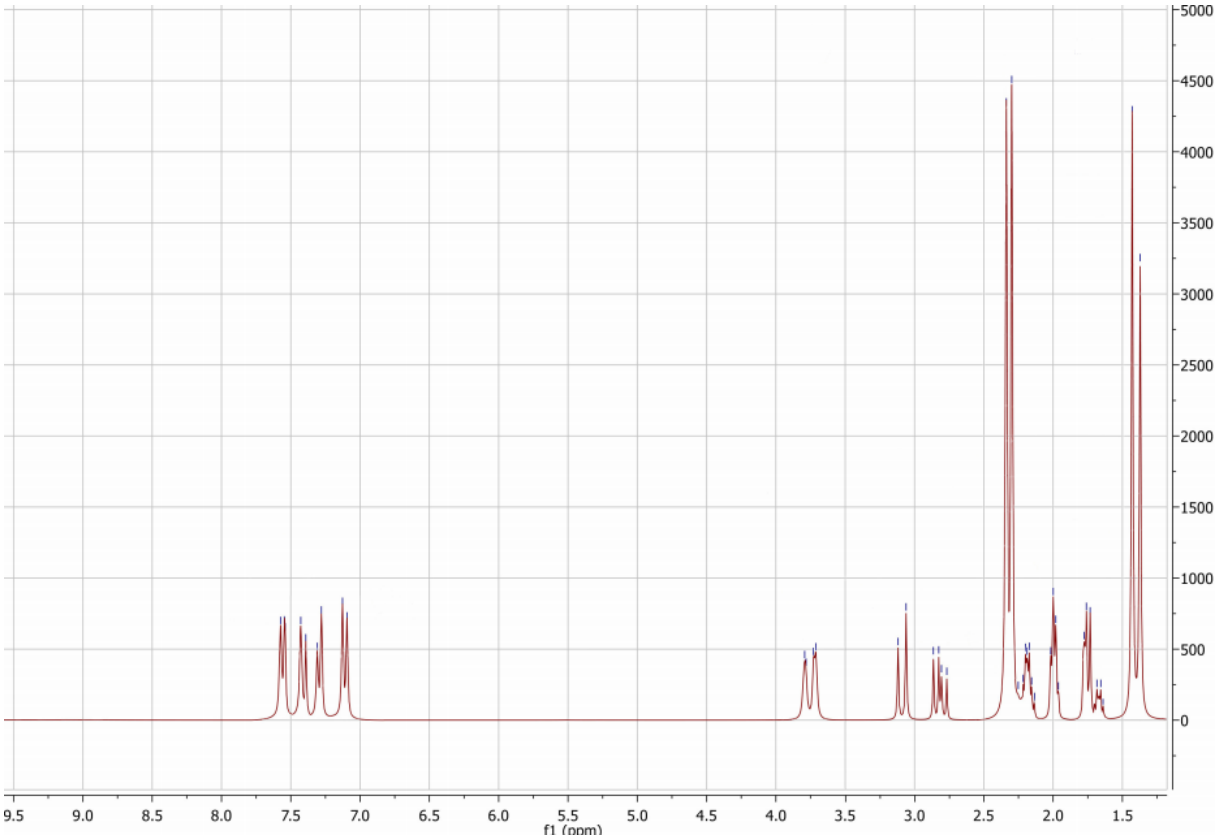

^{1}H NMR spectrum

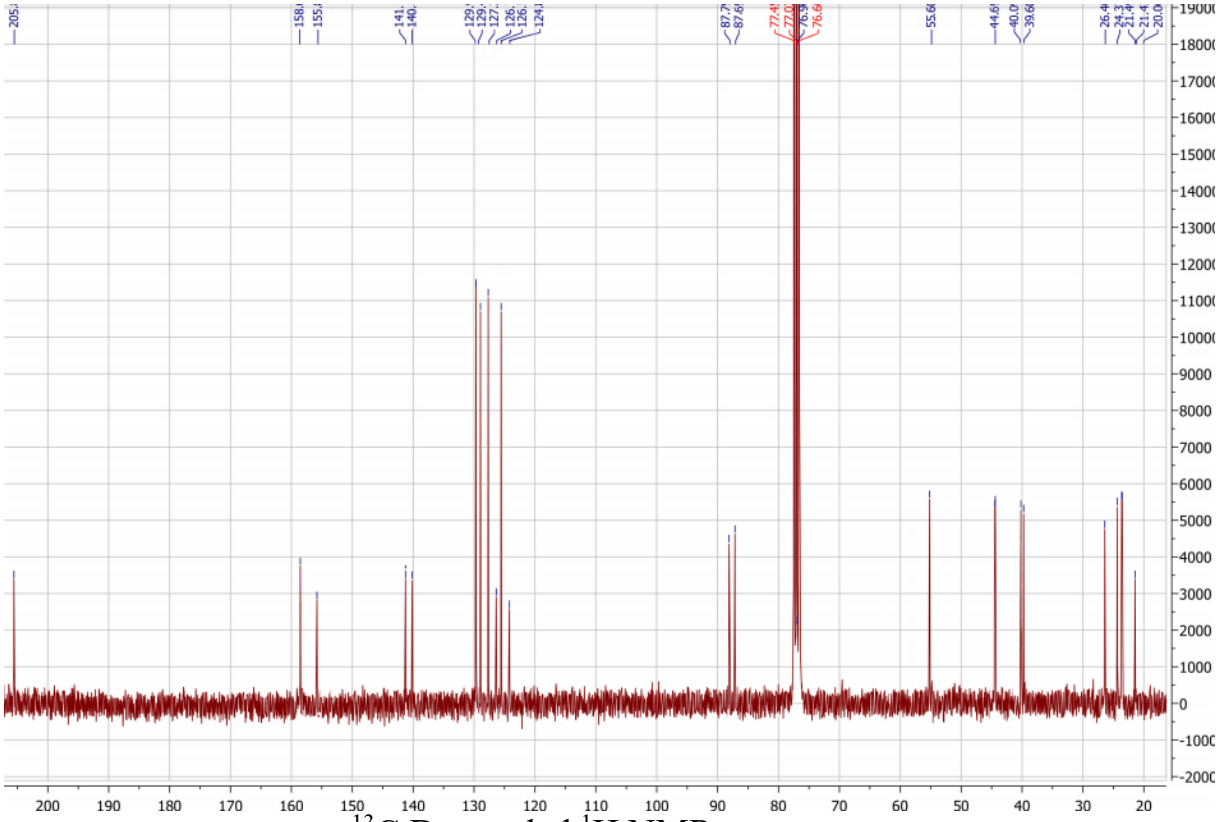

^{13}C Decoupled ^{1}H NMR spectrum

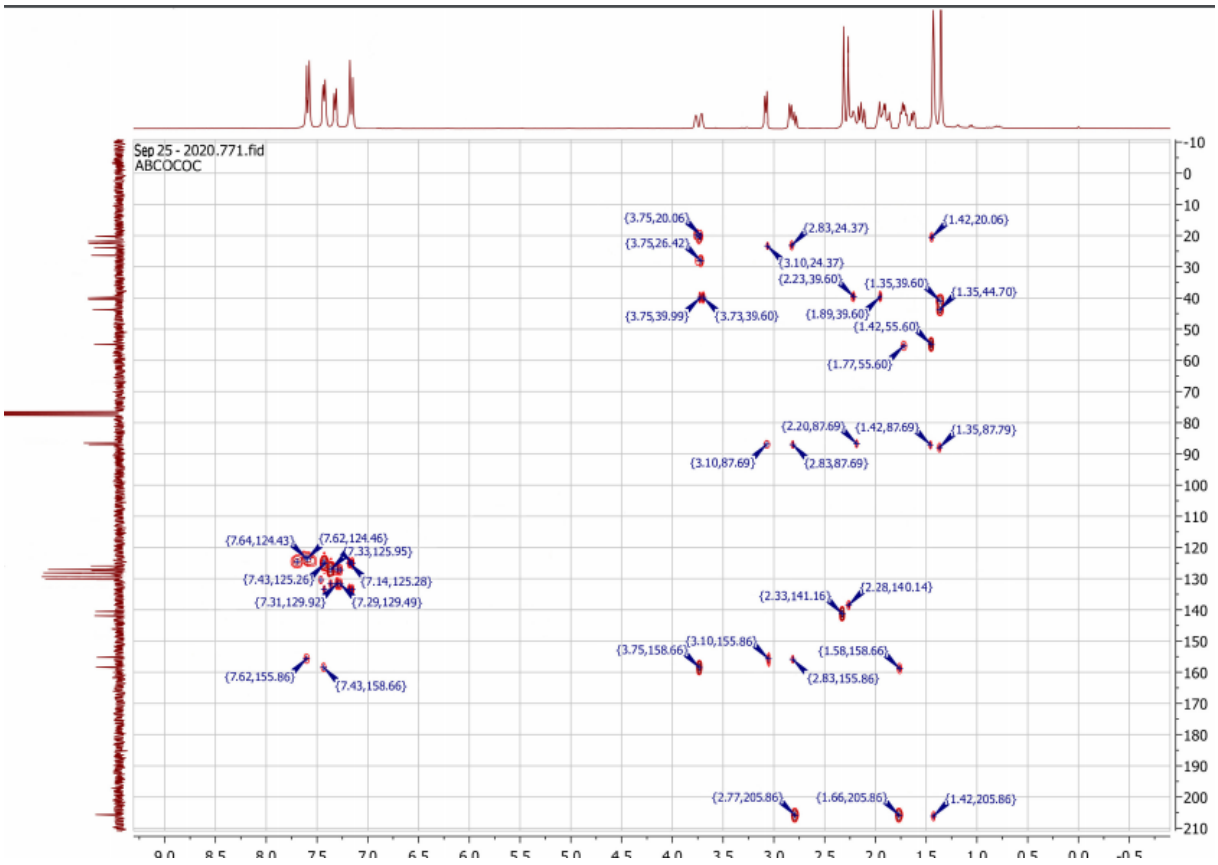

HRMS spectrum

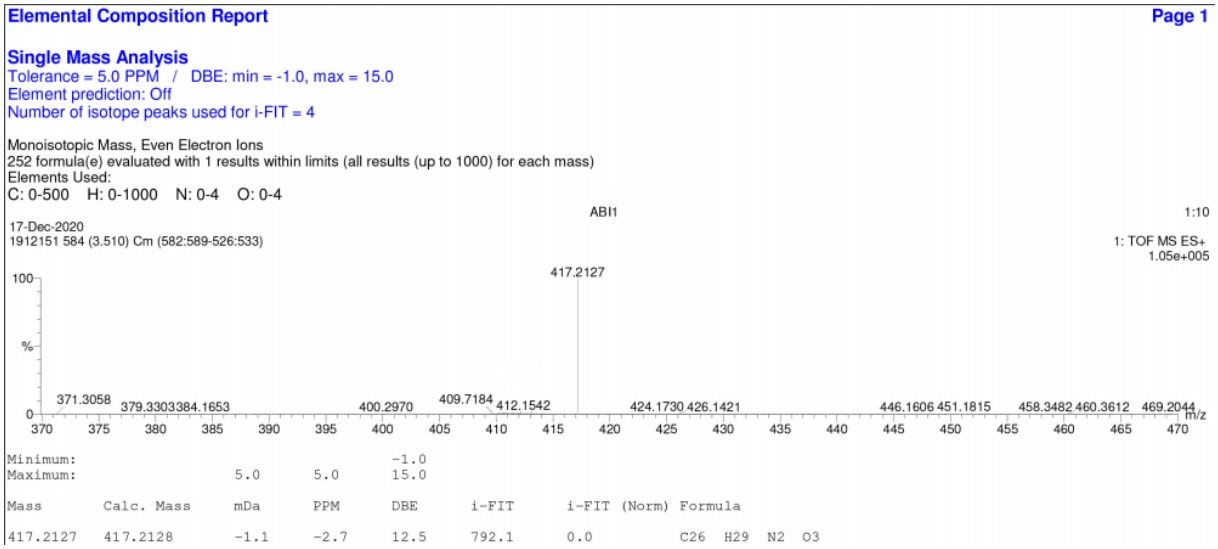

HRMS spectrum

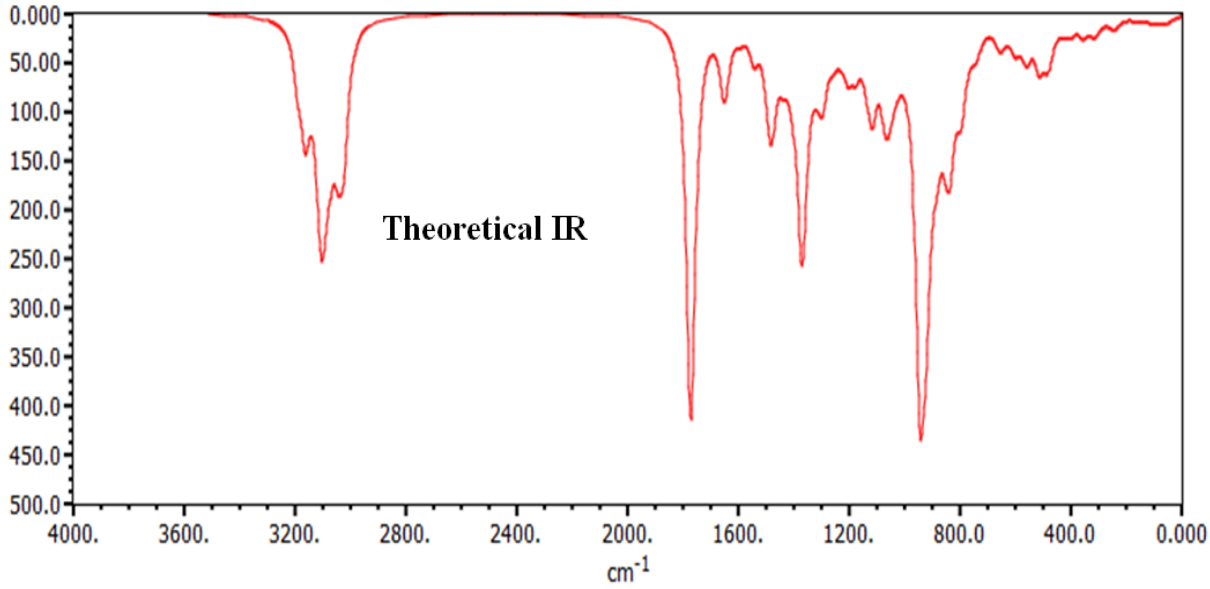

IR spectrum

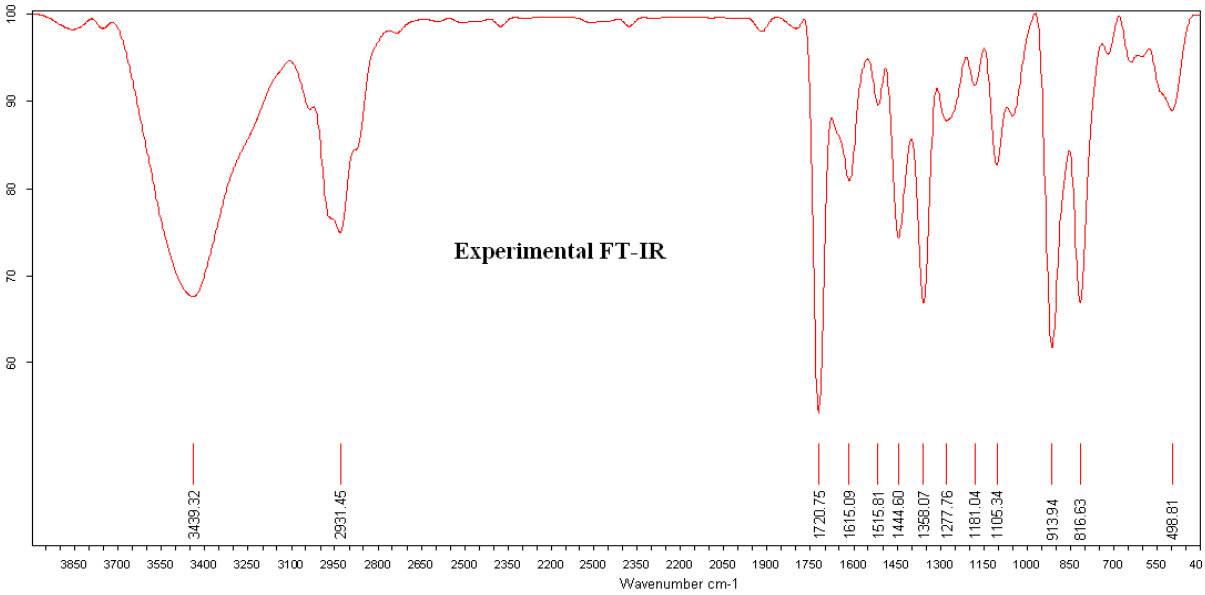

IR spectrum

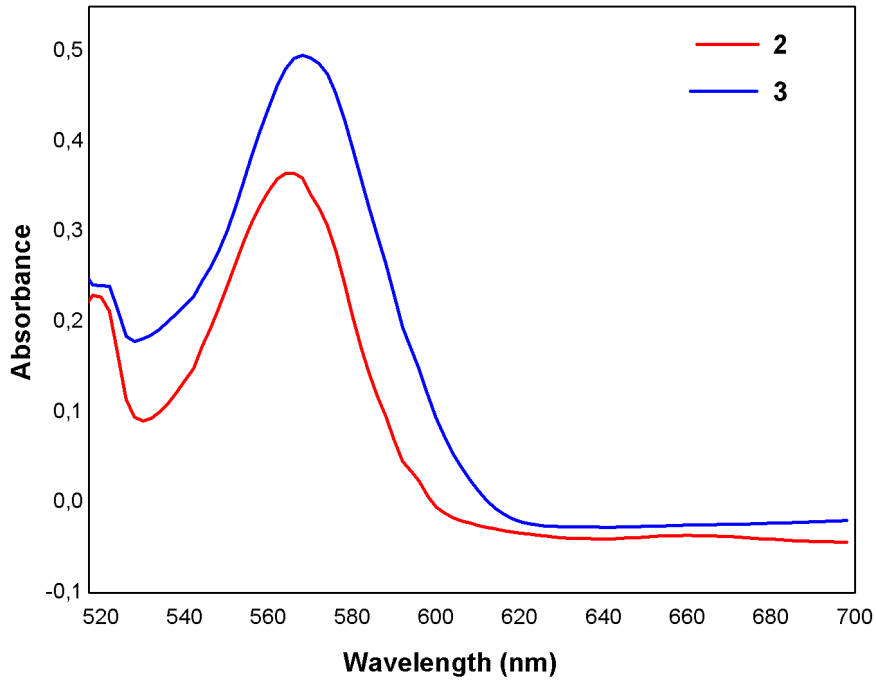

UV spectrum